U.S. Department of the Interior
U.S. Geological Survey

Prepared in cooperation with the
Rockdale County Department of Water Resources

Scientific Investigations Map 3523
Sheet 1 of 2

Estimation of Reservoir Storage Capacity and Geomorphic Change Detection Analysis From a Multibeam Bathymetric Survey of Randy Poynter Lake, Rockdale County, Georgia

By

Amanda R. Whaling and Wesley J. Bolton

2024

Abstract

Rockdale County Department of Water Resources has a directive to update estimates of the reservoir storage capacity of Randy Poynter Lake, located in northern Georgia, and to assess recent sedimentation and associated storage capacity loss. In 2022, the U.S. Geological Survey completed a multibeam bathymetric survey of Randy Poynter Lake to update storage capacity estimates and to quantify storage capacity change since the first multibeam bathymetric survey in 2012 in consideration of estimated errors inherent to bathymetric surveys. Data from the 2022 survey were used to generate contours of the reservoir as well as compute storage capacity at regular increments of water-surface elevation. Storage capacity comparisons between 2012 and 2022 at Randy Poynter Lake show minimal changes that are within the estimated uncertainties, with consistent or slightly increased storage capacities observed at most water-surface elevations and reductions observed at the remaining few elevations. Comparison of the multibeam bathymetric data collected in 2012 with data collected in 2022 further allowed for a formal geomorphic change detection analysis to map, quantify, and infer causation of morphological change over time with respect to a level of detectable change. The volume change in Randy Poynter Lake for the decade between 2012 and 2022 was slightly net-depositional and within the estimated uncertainty. The spatial distribution of sediment deposition was primarily concentrated in the northern portion of the lake, where the principal tributary flows into Randy Poynter Lake. The results of the geomorphic change analysis were used to further understand the future implications to storage capacity change. Despite the challenges of confirming systematic biases because of uncertainties exceeding the observed changes, insights from the study help predict long-term reservoir sediment accumulation, indicating a reservoir half-life extending about 650 years from 2022 on the basis of the current sediment yield estimates.

Introduction

Sediment discharged into Randy Poynter Lake located in Rockdale County, northern Georgia (fig. 1), originates from sources such as Big Haynes Creek and its tributaries, shoreline erosion, and runoff from precipitation events. Sediment settles to the reservoir bottom and decreases the storage capacity of the lake over time if the sediment remains trapped (Schleiss and others, 2016). The construction of Jack Turner Dam and concurrent impoundment of Big Haynes Creek created Randy Poynter Lake circa 1994 to meet the water-supply needs of Rockdale County through the year 2030 (Rockdale Water Resources, 2023), and sediment accumulation is cited as a growing concern according to local news sources (Queen, 2022) as storage capacity decreases.

The storage capacity of Randy Poynter Lake was previously determined from reservoir topobathymetry in turn derived from multibeam echosounder (MBES) and light detection and ranging (lidar) surveys completed in July and August 2012 by the U.S. Geological Survey (USGS) (Lee, 2013), about 18 years after the construction of Jack Turner Dam. Rockdale County Department of Water Resources has a directive to update previous estimates of the storage capacity of Randy Poynter Lake and to understand the extent of recent sediment accumulation. In 2022, the USGS completed a multibeam bathymetric survey of Randy Poynter Lake in cooperation with the Rockdale County Department of Water Resources to update storage capacity estimates below the flood pool elevation of 225.52 meters (m) or 739.90 feet (ft) above the North American Vertical Datum of 1988 (NAVD 88) (Rockdale Water Resources, 2023) and to quantify the storage capacity change since 2012.

Updated bathymetric data for Randy Poynter Lake were collected between November 29 and December 4, 2022, using methodologies for MBES surveys like those described by Huizinga (2017). Raw data were post-processed with HYPACK software (Xylem, 2022) and attributed with uncertainty estimates determined by the Combined Uncertainty and Bathymetric Estimator (CUBE) algorithm (Calder and Wells, 2007). The post-processed data were exported at a reduced spatial density based on a regular grid spacing, wherein each cell in the grid is assigned an elevation and uncertainty value. The gridded elevations were used to generate a three-dimensional surface representation, or digital elevation model (DEM), of Randy Poynter Lake (James and others, 2012). Areas not included in the bathymetric survey and below the flood pool elevation were supplemented with other sources of topobathymetric data to improve DEM definition, discussed in greater detail in the section titled “Contour Map Generation and Storage Capacity Estimation.” The final DEM of Randy Poynter Lake was used to generate contours below the flood pool elevation at regular 0.50 m (~1.64 ft) increments of water-surface elevation as well as compute storage capacity at regular 1-ft (~0.30-m) and 1-m (~3.28-ft) increments of water-surface elevation.

Storage capacity estimates from 2012 and 2022 were compared to determine the storage capacity change since 2012, and comparison of the MBES data collected in 2012 with MBES data collected in 2022 further allowed for a formal geomorphic change detection (GCD) analysis; GCD analysis involves the subtraction of successive DEMs on a cell-by-cell basis to map, quantify, and infer causation of morphological change over time with respect to a level of detectable change (Anderson, 2018; James and others, 2012; Wheaton and others, 2010). The spatial distribution and volume of sediment accumulation in Randy Poynter Lake was determined for the decade between 2012 and 2022 in consideration of estimated errors inherent to bathymetric surveys. The results of the GCD analysis were used to quantify sediment accumulation and to understand the future implications to storage capacity change in Randy Poynter Lake.

The programming language R (R Core Development Team, 2023) has geospatial analysis capabilities comparable to commercial geographic information system platforms and was used for all computations related to DEM and contour generation, storage capacity estimation, GCD analysis, and uncertainty propagation. Gridded bathymetric data collected in 2022 and generated contours are available from Bolton and Whaling (2023) alongside detailed documentation of data collection and post-processing procedures.

This report documents the estimation of reservoir storage capacity and geomorphic change detection analysis from the multibeam bathymetric survey of Randy Poynter Lake completed in 2022 and the determination of storage capacity change from 2012 to 2022. In addition, future impacts of sedimentation on storage capacity loss are assessed by computing the reservoir half-life.

Methods

Bathymetric Data Collection

Full bathymetric coverage of Randy Poynter Lake was collected between November 29 and December 4, 2022, for elevations below approximately 222.50 m (729.99 ft) above NAVD 88 using a marine-based mapping system (MBMS) (Huizinga, 2017). The MBMS operates with several components: the MBES to measure water depths, an inertial navigation system (INS) to georeference the water depths in three-dimensional space, and a data acquisition computer to integrate the data from the MBES and INS in real time. Bathymetric data were collected using the Norbit iWBMSh MBES mounted to a 21-ft boat with the other components of the MBMS (fig. 2) along transects roughly parallel to the shore. Mapping transects maintained a 100-percent overlap and were initiated at the southern end of the reservoir on November 30, 2022, moving further north each day. The Norbit MBES has a curved receiver array that enables bathymetric data to be collected throughout a swath range of 210 degrees. Optimum data are typically collected in a swath of less than 160 degrees (80 degrees on each side of nadir, or straight down below the MBES). The swath was electronically rotated to either side of nadir, improving data collection along the shoreline and in areas less than 2.5 m deep, the practical limit of reasonable and safe data collection with the MBES. To account for the effect of the speed of sound in water on the depth measurements, a sound velocity sensor mounted at the MBES was used to collect continuous measurements of sound velocity. The software onboard the MBES used the sensor data to correct the depths in real time for near-water surface fluctuations in sound velocity. A Valeport mini-SVP was used to collect sound-velocity profiles at roughly hourly intervals throughout the survey to correct the depths for expected changes in sound velocity with respect to depth. The location and time of each profile was recorded to allow for a spatiotemporal interpolation of sound velocity throughout the survey area and subsequent depth correction during post-processing.

The Applanix OceanMaster Position Orientation System for Marine Vessels INS was used to georeference and correct for the pitch, roll, and heading of the MBES. Real-time navigation during the survey used a Differential Global Position System solution improved with real-time kinematic corrections. The real-time data from the INS was further improved in post-processing with POSPac Mobile Mapping Suite (MMS) software (Trimble Applanix, 2022) that utilizes precise ephemeris data imported from a single or network of static Global Navigation Satellite Systems (GNSS) base station(s). A GNSS base receiver was set up over a monumented benchmark on the dam, and it collected static data for an average of 9 hours per day for a total of six base station files. Each file was processed through the Online Positioning User Service (OPUS) (National Geodetic Survey, 2022) to acquire a post-processed benchmark coordinate and elevation as well as several quality-assurance metrics; each processed coordinate solution meets Level I survey-grade GNSS quality requirements according to Rydlund and Densmore (2012). The average of the OPUS solutions was used for the benchmark coordinate in POSPac MMS software as follows: latitude 33°43′49.75176″ N, longitude 83°56′08.48018″ W, and 198.0033 m (ellipsoidal height, referenced to the 1980 Geodetic Reference System). A local base station was chosen to minimize baseline length as opposed to sourcing static base station data from a permanent network of base stations accessible from POSPac MMS, all of which were located several tens of kilometers away from the survey area. The static base station data were applied to the respective day of the real-time INS data collection in POSPac MMS, and the improved navigation solution, called a smoothed best estimate of trajectory, was computed for each day (Bolton and Whaling, 2023).

Four different quality-assurance tests were performed during the bathymetric survey. First, a patch test was used to check for subtle variations in the angular orientation (yaw, pitch, and roll), positional offsets, and timing (latency) of the MBES with respect to the INS (Huizinga, 2017). Transects for the patch test were collected on November 29, 2022, near the dam and involved methodically collecting swaths of data over bathymetric features ideally chosen to identify and quantify orientation offsets for later determination and application in post-processing (section “Bathymetric Data Post-Processing”). Second, reference surface and beam-angle check transects were collected as a part of a beam angle test to determine the accuracy of the water depths obtained by the outer beams of the MBES (U.S. Army Corps of Engineers, 2013). A preliminary comparison between the reference and check data indicated the central 120 degrees of the MBES swath sector averaged less than 2 centimeters (cm) (absolute value) out to 60 degrees from nadir; therefore, data collection was limited to 120 degrees for the duration of the survey. The swath sector was extended to 150 degrees when the electronic tilt was enabled to maximize coverage for mapping shoreline and shallow areas. The beam-angle test was later reprocessed to ensure the post-processed data did not require exclusion of additional outer beams within the 120-degree sector from nadir (section “Bathymetric Data Post-Processing”). The third test, called a cross-check analysis, is useful for quantifying the uncertainty associated with grid resolution choice in the final gridded bathymetric dataset (section “Storage Capacity Uncertainty”). The cross-check test involved collection of a 300-m transect each day that “crosses” previously collected data to independently “check” against the final gridded bathymetric dataset, provided that the cross-check transect data remain in the original resolution acquired during the survey and are excluded from generation of the final gridded bathymetric dataset. Lastly, two reference surfaces in the deepest part of the reservoir were collected at two different MBES frequencies—200 and 400 kilohertz (kHz)—to determine if a higher frequency could be used without biasing the comparison with the 2012 baseline bathymetric survey data, which were primarily collected with a MBES operated at 300 kHz (Lee, 2013). Cross-sectional profiles were drawn across the reference surfaces, and the elevations along the profile were compared. No systematic differences were found between the frequencies; therefore, the MBES was operated at 400 kHz for the duration of the survey.

Bathymetric Data Post-Processing

HYPACK software was used for processing all data from the bathymetric survey. Data were processed to a grid area divided into 0.50- x 0.50-m (~1.64- x 1.64-ft) grid cells. Smoothed best estimate of trajectory files generated by and exported from POSPac MMS software were applied to the respective day of data collection. The sound velocity profiles, corrected for erroneous measurements, were applied to each sounding on the basis of an interpolated profile determined by geographic position and time of day. Daily draft values were entered into HYPACK to properly apply measured sound velocity from the MBES up to the water surface. Following the post-processing, corrections were acquired and applied from the patch test in HYPACK for roll, pitch, yaw, and latency (Bolton and Whaling, 2023). The beam-angle test was reprocessed, and the results indicated the initial test was valid, with an improved average difference of less than 1 cm (absolute value) out to 65 degrees from nadir. The data were cleaned with a combination of automatic filtering algorithms implemented in HYPACK and qualitative inspection, such as the deletion of any points that were isolated from the points composing the reservoir bottom. Any remaining vertical objects were manually removed, mostly upright trees not cleared prior to lake impoundment. Removal of trees ensured that derivative DEMs generated from the data were not biased high, which occurred when the width of the vertical object was narrower than the grid cell resolution during conversion of raw point data to a gridded dataset with regular grid spacing.

Total propagated uncertainty was estimated in HYPACK for each depth on the basis of known, estimated, or parameterized uncertainties associated with the various components of the MBMS and environmental factors. The CUBE algorithm implemented in HYPACK then uses the total propagated uncertainty estimates along with the remaining random variability in the post-processed depths to generate final depths attributed with an uncertainty for each cell in the grid (Calder and Wells, 2007). Post-processed bathymetric data were exported from HYPACK in units of meters referenced to NAVD 88, GEOID 12B, and projected in Universal Transverse Mercator (UTM) coordinates. UTM zone 16 north was strategically chosen for data processing and export, despite Randy Poynter Lake being physically located in UTM zone 17 north, to facilitate intermediary comparisons with 2012 data, which were projected in UTM zone 16 north. Similarly, GEOID 12B was chosen to facilitate integration of the 2022 survey data with aerial lidar data referenced to NAVD 88, GEOID 12B (section “Contour Map Generation and Storage Capacity Estimation”). Lastly, a script was written in the R language (R Core Development Team, 2023) which imports the gridded CUBE elevations and uncertainties from each day, merges the data into one combined dataset, and subsets the data only to having CUBE uncertainty values less than 1.0 m (~3.28 ft); CUBE uncertainty values exceeding this magnitude were rare, although they can be more frequent in areas having a steep slope, such as channel margins or rocky shorelines. In fact, CUBE uncertainty values for more than 99 percent of points were less than 0.15 m (~0.49 ft), which is within the specifications for a “Special Order” survey, the most-stringent survey standard of the International Hydrographic Organization (International Hydrographic Organization, 2020). The final bathymetric dataset was projected to UTM zone 17 north and exported as an Esri Shapefile (Esri, 1998) from R, provided with position data in three dimensions and units of meters horizontally referenced to the North American Datum of 1983, 2011 realization (NAD 83 2011), and vertically referenced to NAVD 88, GEOID 12B (Bolton and Whaling, 2023).

Contour Map Generation and Storage Capacity Estimation

The gridded 2022 dataset of reservoir-bottom elevations was combined with additional topobathymetric data outside of the area collected by the MBMS, with elevations above about 222.5 m (~730 ft) above NAVD 88 and up to the flood pool elevation. The supplemental data include topographic bare-earth aerial lidar data collected during 2018–19, which are publicly available through the USGS 3D Elevation Program (U.S. Geological Survey, 2023a), as well as topographic bare-earth lidar and single-beam data collected by Lee (2013). Using the multisource topobathymetric dataset, a contour at the flood pool elevation was generated in Global Mapper software (Blue Marble Geographics, 2023) and manually closed at Jack Turner Dam, resulting in a geospatial boundary having an aerial coverage of 2.91 square kilometers (km^2), or ~1.12 square miles (mi^2) (flood pool elevation contour, fig. 3). Approximately 2.25 km^2 (~0.87 mi^2) was surveyed in 2022 with the MBMS, composing 77.11 percent of the total area encompassing the closed flood pool extent. A DEM of Randy Poynter Lake up to the flood pool boundary was generated from the multisource topobathymetric dataset at a 1-m (~3.28-ft) resolution using an inverse distance weighting algorithm in R with the “grid_terrain” function from the *lidR* package (Roussel and Auty, 2023) to create a continuous surface. A 1-m cell size was used in consideration of different point densities between the sources of data. Topobathymetric contours were created from the DEM in R with the “as.contour” function from the *terra* package (Hijmans, 2023) at 0.50-m (~1.64 ft) elevation increments (bathymetric contours, fig. 3). The contours were further edited in Global Mapper software, particularly near Jack Turner Dam, where open contours were manually closed.

A function was written in R to take the multisource DEM of Randy Poynter Lake and iterate over user-specified water-surface elevation increments for a given range and compute the storage capacity and areal extent of the reservoir. The function was used to compute updated storage capacity in volumetric units of acre-feet and cubic meters at 1-ft (~0.30-m) and 1-m (~3.28-ft) elevation increments over the range from 210.00 m (~688.98 ft) to 225.00 m (~738.19 ft) above NAVD 88, as well as for the normal and flood pool elevations (table 1). Reservoir areal extent was computed in units of square meters for each water-surface elevation increment by multiplying the DEM grid cell area (1 m^2; 10.76 ft^2) by the number of cells having elevation values below the given elevation increment. Areal extent is not reported herein but was stored for computation of storage capacity uncertainty.

Table 1. Reservoir storage capacities and uncertainties for Randy Poynter Lake at specified water-surface elevations in 2022 and the change in storage capacity and storage capacity loss since 2012.

[NAVD 88, North American Vertical Datum of 1988; X, value not computed for the specified water-surface elevation; %, percent]

Water-surface elevation, in meters above NAVD 88	Water-surface elevation, in feet above NAVD 88	2022 storage capacity ($s_{2022, WSEL}$), in cubic meters	2022 storage capacity uncertainty ($\sigma s_{2022, WSEL}$), in cubic meters (95% confidence level)	2022 storage capacity ($s_{2022, WSEL}$), in acre-feet	2022 storage capacity uncertainty ($\sigma s_{2022, WSEL}$), in acre-feet (95% confidence level)	Change in storage capacity since 2012 (Δs_{WSEL}), in acre-feet	Change, in storage capacity (L_{WSEL}), in percent
210.00	688.98	383,871.30	75,557.00	311.21	61.26	X	X
210.31	690.00	488,923.09	84,664.55	396.38	68.64	16.38	4.31
210.62	691.00	603,517.09	94,350.32	489.28	76.49	9.28	1.93
210.92	692.00	732,102.02	106,725.81	593.52	86.52	13.52	2.33
211.00	692.26	767,553.98	109,746.90	622.27	88.97	X	X
211.23	693.00	876,360.64	118,502.37	710.48	96.07	20.48	2.97
211.53	694.00	1,035,963.47	130,785.27	839.87	106.03	19.87	2.42
211.84	695.00	1,210,759.62	142,498.03	981.58	115.53	21.58	2.25
212.00	695.54	1,311,034.29	149,694.04	1,062.87	121.36	X	X
212.14	696.00	1,401,893.80	156,451.32	1,136.53	126.84	26.53	2.39
212.45	697.00	1,610,292.84	169,039.87	1,305.49	137.04	25.49	1.99
212.75	698.00	1,834,904.91	181,746.25	1,487.58	147.34	27.58	1.89
213.00	698.82	2,030,490.69	191,623.65	1,646.15	155.35	X	X
213.06	699.00	2,075,502.33	193,618.75	1,682.64	156.97	32.64	1.98
213.36	700.00	2,330,490.22	204,410.73	1,889.36	165.72	29.36	1.58
213.67	701.00	2,599,245.62	215,473.86	2,107.24	174.69	37.24	1.80
213.97	702.00	2,882,237.23	226,570.31	2,336.67	183.68	36.67	1.59
214.00	702.10	2,910,835.68	227,694.86	2,359.85	184.60	X	X
214.27	703.00	3,180,061.86	238,887.01	2,578.12	193.67	38.12	1.50
214.58	704.00	3,493,696.79	250,849.96	2,832.39	203.37	32.39	1.16
214.88	705.00	3,822,444.22	262,748.64	3,098.91	213.01	38.91	1.27
215.00	705.38	3,951,049.49	267,048.54	3,203.17	216.50	X	X
215.19	706.00	4,166,168.21	274,103.62	3,377.57	222.22	37.57	1.12
215.49	707.00	4,523,789.60	284,183.12	3,667.50	230.39	37.50	1.03
215.80	708.00	4,893,617.92	293,528.96	3,967.32	237.97	47.32	1.21
216.00	708.66	5,144,359.47	299,957.25	4,170.60	243.18	X	X
216.10	709.00	5,275,694.53	303,416.59	4,277.08	245.98	47.08	1.11
216.41	710.00	5,670,520.28	313,300.42	4,597.17	254.00	47.17	1.04
216.71	711.00	6,077,975.56	323,278.04	4,927.49	262.09	47.49	0.97
217.00	711.94	6,473,468.77	333,586.79	5,248.13	270.44	X	X
217.02	712.00	6,498,767.28	334,293.79	5,268.64	271.02	48.64	0.93
217.32	713.00	6,934,564.94	346,558.83	5,621.94	280.96	41.94	0.75
217.63	714.00	7,385,866.78	358,142.81	5,987.82	290.35	47.82	0.81
217.93	715.00	7,851,822.77	369,778.69	6,365.58	299.78	45.58	0.72
218.00	715.22	7,957,152.20	372,435.80	6,450.97	301.94	X	X
218.24	716.00	8,332,915.81	381,587.15	6,755.60	309.36	45.60	0.68
218.54	717.00	8,828,579.16	392,594.33	7,157.45	318.28	37.45	0.53
218.85	718.00	9,338,358.23	403,712.44	7,570.73	327.30	40.73	0.54
219.00	718.50	9,599,903.17	409,330.90	7,782.77	331.85	X	X
219.15	719.00	9,862,433.26	414,984.10	7,995.60	336.43	35.60	0.45
219.46	720.00	10,401,045.60	426,342.41	8,432.26	345.64	42.26	0.50
219.76	721.00	10,954,164.11	437,709.76	8,880.69	354.86	40.69	0.46
220.00	721.78	11,397,697.97	446,716.61	9,240.26	362.16	X	X
220.07	722.00	11,521,968.07	449,178.53	9,341.01	364.15	41.01	0.44
220.37	723.00	12,104,673.57	461,173.38	9,813.42	373.88	33.42	0.34
220.68	724.00	12,703,112.62	473,682.18	10,298.58	384.02	−1.42	−0.01
220.98	725.00	13,317,729.22	486,346.91	10,796.86	394.29	−3.14	−0.03
221.00	725.06	13,357,719.36	487,134.85	10,829.28	394.93	X	X
221.29	726.00	13,948,519.37	498,952.83	11,308.25	404.51	8.25	0.07
221.59	727.00	14,595,463.79	511,663.98	11,832.73	414.81	32.73	0.28
221.89	728.00	15,260,007.02	526,387.12	12,371.49	426.75	71.49	0.58
222.00	728.34	15,493,530.37	530,881.50	12,560.81	430.39	X	X
222.20	729.00	15,942,266.71	539,338.22	12,924.61	437.25	24.61	0.19
222.50	730.00	16,641,086.13	552,064.60	13,491.15	447.57	91.15	0.68
222.81	731.00	17,355,523.39	563,794.74	14,070.35	457.08	70.35	0.50
223.00	731.63	17,810,063.45	570,581.78	14,438.85	462.58	X	X
223.11	732.00	18,084,347.04	574,418.19	14,661.22	465.69	61.22	0.42
223.42	733.00	18,826,104.93	584,113.95	15,262.57	473.55	62.57	0.41
223.72	734.00	19,579,991.26	593,460.26	15,873.76	481.13	73.76	0.47
224.00	734.91	20,274,026.38	602,434.27	16,436.42	488.40	X	X
[1]224.03	[1]735.00	20,346,089.79	603,691.17	16,494.84	489.42	−5.16	−0.03
225.00	738.19	22,942,659.65	664,301.02	18,599.92	538.56	X	X
[2]225.52	[2]739.90	24,426,825.51	686,334.20	19,803.15	556.42	X	X

[1]Normal pool elevation.

[2]Flood pool elevation.

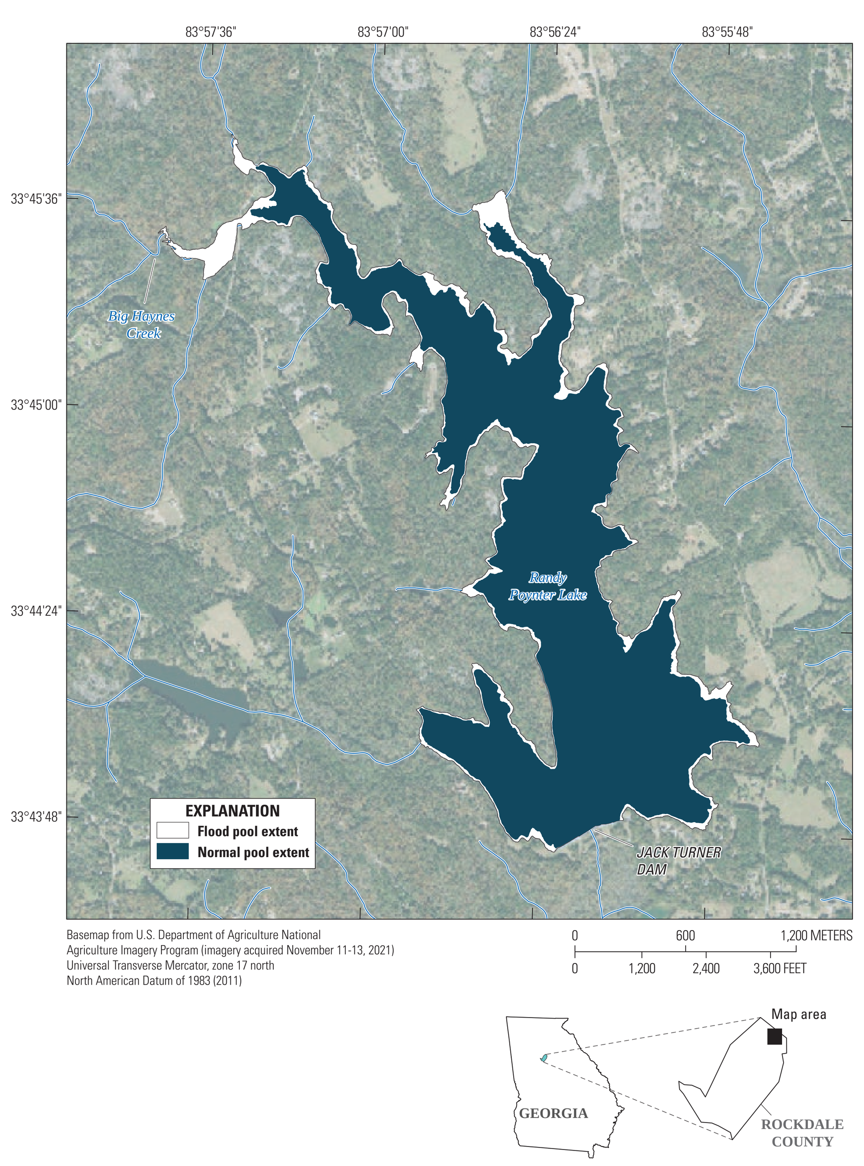

Figure 1. Study area including flood pool and normal pool areal extents of Randy Poynter Lake, Rockdale County, Georgia.

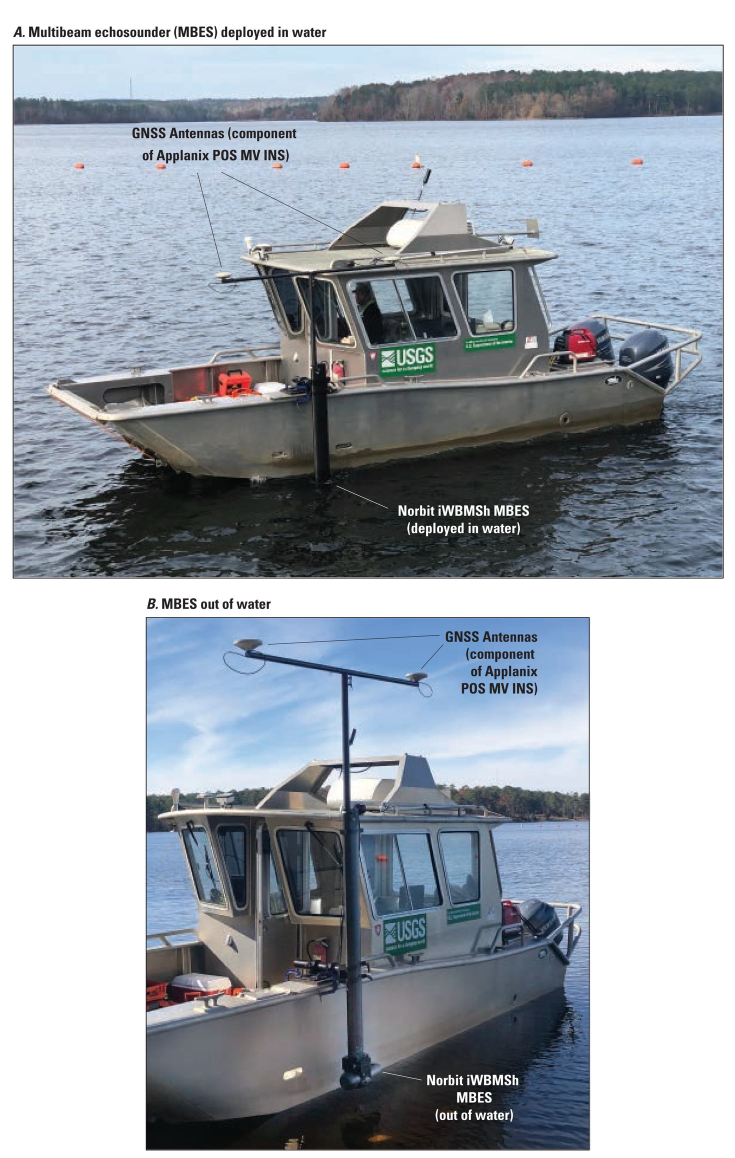

Figure 2. Multibeam echosounder (MBES) *A*, deployed in the water and, *B*, out of the water and components of the Applanix Position Orientation System for Marine Vessels (POS MV) inertial navigation system (INS) mounted to a 21-foot boat, including Global Navigation Satellite System (GNSS) antennas. Photographs by Amanda Whaling, U.S. Geological Survey.

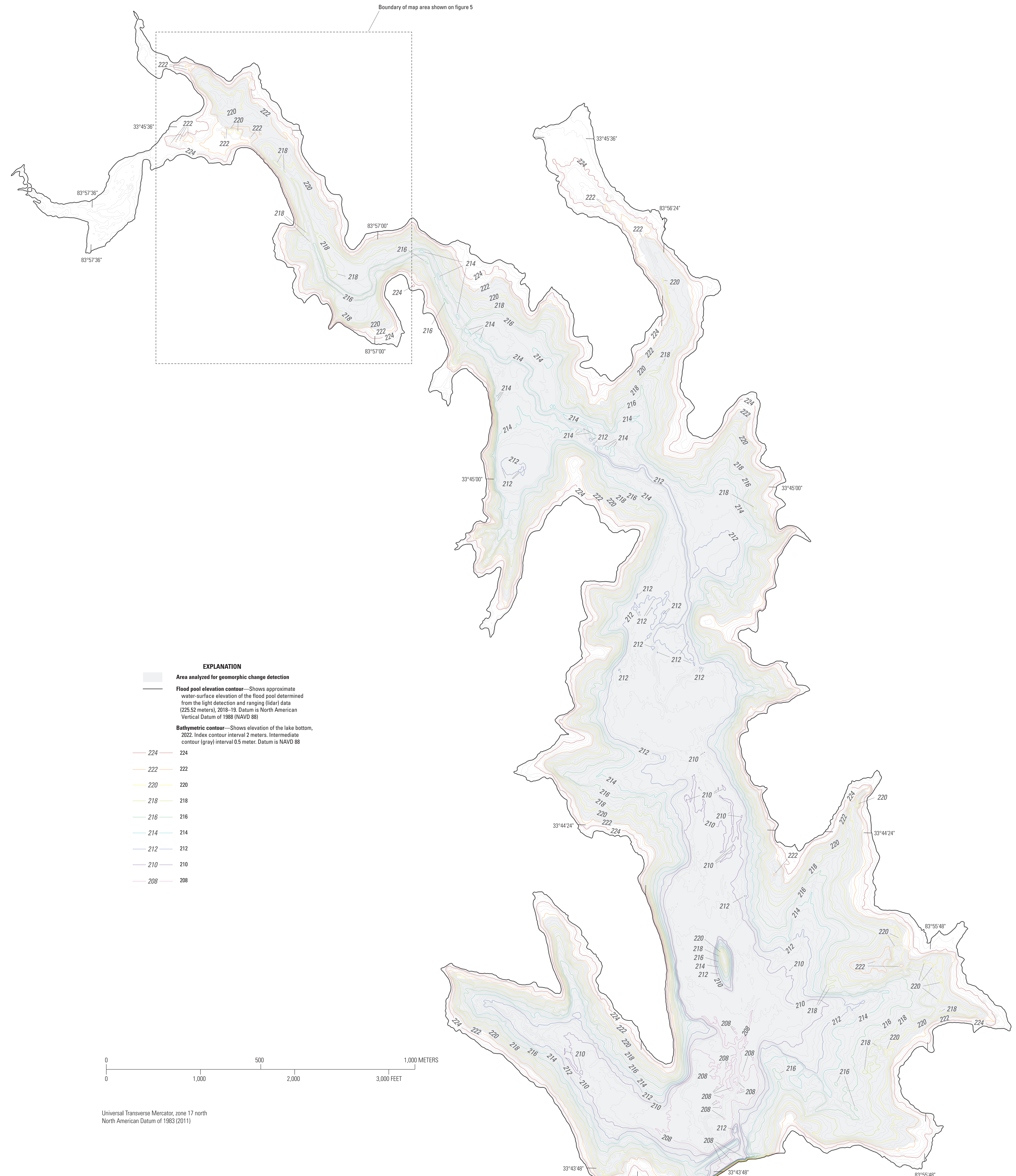

Figure 3. Updated topobathymetric contours of Randy Poynter Lake derived from a continuous digital elevation model (DEM). Data used to generate the DEM primarily originate from the 2022 bathymetric survey and are available in Bolton and Whaling (2023).

Any use of trade, firm, or product names is for descriptive purposes only and does not imply endorsement by the U.S. Government

For sale by U.S. Geological Survey, Information Services, Box 25286, Federal Center, Denver, CO 80225, 1–888–ASK–USGS

Digital files available at https://doi.org/10.3133/sim3523

Suggested citation: Whaling, A.R., and Bolton, W.J., Estimation of reservoir storage capacity and geomorphic change detection analysis from a multibeam bathymetric survey of Randy Poynter Lake, Rockdale County, Georgia: U.S. Geological Survey Scientific Investigations Map 3523, 2 sheets, https://doi.org/10.3133/sim3523.

Associated data for this publication: Aulenbach, B.T., Henley, J.C., and Hopkins, K.G., 2023, Watershed characteristics and streamwater constituent load data, models, and estimates for 15 watersheds in Gwinnett County, Georgia, 2000–2021: U.S. Geological Survey data release, https://doi.org/10.5066/P9G8HZTY.

Bolton, W.J., and Whaling, A.R., 2023, Bathymetric and supporting data for estimation of reservoir storage capacity and geomorphic change detection analysis from a multibeam bathymetric survey of Randy Poynter Lake, Rockdale County, Georgia: U.S. Geological Survey data release, https://doi.org/10.5066/P9G9YVDU.

ISSN 2329-132X (online)
https://doi.org/10.3133/sim3523

Prepared in cooperation with the
Rockdale County Department of Water Resources

Geomorphic Change Detection

Data Preparation

Data preparation in the context of GCD primarily involves ensuring data from repeat surveys are directly comparable while also minimizing degradation of the original datasets that can potentially occur, such as by resampling. Datum and projection consistency are especially important in that regard; all data were compared using the same horizontal and vertical datum and realization, geoid model, and projection. Minor vertical datum discrepancies were assumed to be present and duly accounted for in uncertainty computations (section "Geomorphic Change Detection Uncertainty").

Two DEMs were created from the 2012 and 2022 MBES datasets for the purpose of GCD analysis using the "grid_terrain" function from the *lidR* package (Roussel and Auty, 2023) in the R environment. Specifically, the grid resolution and origin used for processing and export in HYPACK were used to recreate a 0.50- x 0.50-m (~1.64- x 1.64-ft) grid for DEM generation and GCD analysis; this procedure ensured resampling did not occur when converting the points in the 2022 dataset to a DEM. The same grid was used to extract the cell median from a triangulated irregular network (TIN) created from the 2012 gridded TIN points. Regeneration of the TIN was necessary to remove areas unsuitable for GCD analysis based on visual inspection of the 2012 TIN in Global Mapper software; such areas were characterized by abrupt changes in elevation interpreted to be TIN interpolation or data-processing artifacts. TIN interpolation was used in place of the removed areas, which totaled roughly 0.04 km² (~0.015 mi²), about 1.77 percent of the total area analyzed for geomorphic change. Lastly, grid node locations without elevations present for either the 2012 or 2022 DEM were removed, resulting in two final DEMs directly comparable for GCD. The area of GCD analysis is approximately 2.22 km² (~0.86 mi²), or 76.63 percent of the closed-contour flood pool extent (fig. 3); all data within this area originate from the MBES surveys.

Bathymetric Change and Difference Map

The 2012 DEM used for GCD analysis was subtracted from the 2022 DEM to determine the bathymetric change (Δz) on a cell-by-cell basis (Ghoshal and others, 2010; James and others, 2012), formulated by equation 1:

$$\Delta z = z_{2022} - z_{2012}, \tag{1}$$

where

- z_{2022} represents the 2022 gridded elevations, and
- z_{2012} represents the 2012 gridded elevations.

The resulting bathymetric change map (fig. 4) shows the spatial representation of net change that occurred over more than a decade. The sign convention of the difference operation in equation 1 dictates that a positive bathymetric difference ($\Delta z > 0$) corresponds to an increase in lake bottom elevation since 2012, and a negative bathymetric difference ($\Delta z < 0$) corresponds to a decrease in lake bottom elevation since 2012. Difference values near zero indicate minimal or no observed bathymetric change since 2012.

Bathymetric change is near zero for most of the survey area. The area with the greatest magnitude of positive bathymetric change is in the northernmost portion of the area analyzed for geomorphic change, and magnitude decreases toward Jack Turner Dam to the southeast. Positive bathymetric change appears to converge to near zero at the 83°57′ west meridian (figs. 3, 4). The spatial pattern of observed bathymetric change aligns with the approximate northwest-to-southeast flow direction of Big Haynes Creek. Further, the location with the greatest magnitude of positive bathymetric change coincides with the inflow location of Big Haynes Creek into Randy Poynter Lake. Therefore, the positive bathymetric change in Randy Poynter Lake is interpreted to be largely a consequence of sediment deposition originating from Big Haynes Creek. The decrease in the magnitude of deposition away (south) from this sediment source is characteristic of deltaic processes wherein sediment-laden streamflow decelerates near the inflow location, resulting in sediment deposition and, over time, the formation of a deposit that tapers out toward the interior of the lake (Coleman and Wright, 1975; Elliott, 1986). Delta formation occurring sometime after the impoundment of Randy Poynter Lake is illustrated by deposition at the inflow of Big Haynes Creek measured by Lee (2013) and comparing pre-impoundment topography with the 2012 topobathymetry.

Volumetric Change

The bathymetric change (fig. 4) expressed as a volume of change, v, is the simple product of the grid-cell depths and areas (Ghoshal and others, 2010) and is formulated by equation 2:

$$v = L^2 \sum_{i=1}^{n} \Delta z_i, \tag{2}$$

where

- L is the grid cell resolution; and
- Δz_i is the bathymetric change at each grid cell, i, in the bathymetric change map (fig. 4) out of the total number of grid cells, n, in the area of analysis.

Equation 2 forms the basis for all volume change computations, including the net volume change, v_{net}, the volume of deposition, v_{dep}, and the volume of erosion, v_{ero}. Logical subsetting in R was used to evaluate equation 2 to determine volume change for the entire area of Randy Poynter Lake analyzed by using GCD, A_{RP} (fig. 3). For the computation of v_{net}, n comprises all grid cells in the survey area; for v_{dep} and v_{ero}, n is restricted to cells with positive bathymetric change ($\Delta z > 0$) and negative bathymetric change ($\Delta z < 0$), respectively.

Volume change was also computed for a subarea of interest within Randy Poynter Lake, A_{BH}, constrained to the northwest portion of the study area (fig. 5) near the inflow location of Big Haynes Creek (figs. 3, 4). The A_{BH} subarea is defined as the area west of the 83°57′ west meridian (figs. 3–5), where bathymetric change appears to be dominated by deposition from sediment discharged into Randy Poynter Lake from Big Haynes Creek. Grid cells located in A_{BH} were extracted using a geospatial clipping operation in R, and logical subsetting was similarly used to evaluate equation 2 to further investigate the spatial distribution of deposition in Randy Poynter Lake. Figure 5 more clearly shows a greater magnitude of deposition for cells near the inflow location of Big Haynes Creek compared to areas farther away.

The estimates for the net volume change as well as the volume of deposition and erosion are reported in table 2 for A_{RP} and A_{BH}. According to the reported net volume change for A_{RP}, the reservoir experienced more deposition on average than erosion, but the volume of change represents less than 1 percent of the total storage capacity of Randy Poynter Lake at the normal pool elevation. The volume change results differ for each area analyzed because bathymetric change is not constant throughout Randy Poynter Lake, as evidenced by fig. 4; about half of all measured deposition in the reservoir occurred in the A_{BH} subarea (v_{dep}, table 2). The average change in each grid cell in A_{RP} is 0.36 cm (~0.011 ft) of deposition and about 38 cm (~1.25 ft) of deposition in A_{BH}.

Uncertainty

Geomorphic Change Detection Uncertainty

Uncertainty estimation and propagation is necessary to interpret estimated bathymetric change. The uncertainty analysis is premised on the expectation that there are errors in the underlying datasets used to map and quantify bathymetric change. Because bathymetric change is quantified in terms of an elevation difference (eq. 1), the error is similarly related in terms of the vertical measurement uncertainty. The main components of the vertical uncertainty are typically uncorrelated random errors, spatially correlated errors, and systematic errors (Anderson, 2018). Random and spatially correlated errors were investigated and determined to be a negligible component of the total uncertainty budget. Only a systematic error in the 2012 and 2022 dataset is used for GCD uncertainty estimation and propagation to account for uncertainty in the measured reservoir-bottom elevations with respect to an absolute vertical datum. Thus, the vertical datum uncertainty in the 2022 dataset, $\sigma z_{2022,DATUM}$, is approximated with the overall root mean square statistic from the OPUS solutions determined from each day of surveying during the 2022 survey campaign (section "Bathymetric Data Collection") and serves as an independent measure of vertical datum uncertainty. The maximum root mean square is used and assumed to be constant throughout the survey area such that $\sigma z_{2022,DATUM} = 0.015$ m (~0.049 ft). Vertical datum uncertainty in the 2012 data is assumed to be of a similar magnitude; therefore, the same value is used for approximation of $\sigma z_{2012,DATUM}$. Other sources of systematic errors are assumed to be negligible. For example, horizontal errors are likely present too and will induce a vertical error over a variable-topography terrain, but the relatively flat reservoir-bottom slope means those errors can reasonably be ignored.

The volumetric uncertainty, σv, given by equation 3 was computed in R and is formulated by combining the systematic errors in quadrature, assuming each is an independent process of the other, times the grid cell area, L^2, times the number of cells, n, in the area of interest, such as A_{RP} or A_{BH}, following guidance outlined by Anderson (2018):

$$\sigma v = nL^2 \sqrt{\sigma z^2_{2012,\,DATUM} + \sigma z^2_{2022,DATUM}}\,. \tag{3}$$

For estimation of σv around an estimate of net volume change (σv_{net}), n is determined from the number of all grid cells in the area of interest; for σv around an estimate of positive volume change (σv_{dep}), n is determined from the number of all grid cells in the area of interest with positive bathymetric change; lastly, for σv around an estimate of negative volume change (σv_{ero}), n is determined from the number of all grid cells in the area of interest with negative bathymetric change.

Using $\sigma z_{2012,DATUM} = \sigma z_{2022,DATUM} = 0.015$ m (~0.049 ft) and following equation 3, σv_{net}, σv_{dep}, and σv_{ero} were estimated for both A_{RP} and A_{BH} and then multiplied by 1.96 to achieve the volume uncertainty at the 95-percent confidence level (table 2). The magnitude of the measured change is within the propagated uncertainty, except for v_{net} computed for A_{RP} (table 2). Net deposition observed in the Big Haynes Creek area, A_{BH}, is greater than the error, and thus, the true volume change can be interpreted to also be net-depositional. In the case of the entire study area, A_{RP}, the true volume change has a value somewhere within the computed uncertainty bounds at the 95-percent confidence level, which includes zero change.

Storage Capacity Uncertainty

Uncertainty in each 2022 storage capacity estimate, $\sigma s_{2022,WSEL}$, for a given water-surface elevation, was computed in R, according to equation 4:

$$\sigma s_{2022,WSEL} = A_{WSEL} \sqrt{\sigma z^2_{2022,\,DATUM} + \sigma z^2_{2022,DEM}}\,. \tag{4}$$

Similar to equation 3, uncertainties relevant to 2022 storage capacity estimation—$\sigma z_{2022,DATUM}$ and $\sigma z_{2022,DEM}$—are added in quadrature and multiplied by the reservoir areal extent, A_{WSEL}, computed for a given water-surface elevation (section "Contour Map Generation and Storage Capacity Estimation"). In addition to the vertical datum uncertainty in the 2022 dataset, a DEM generation error, $\sigma z_{2022,DEM}$, is introduced to account for a systematic error that arises from gridding the 2022 MBES points during post-processing (section "Bathymetric Data Post-Processing"). The DEM generation error is formulated by the root mean square error of randomly selected elevations from the cross-check line points (section "Bathymetric Data Collection") and the elevation value at the same location from the 2022 topobathymetric DEM. Cross-check lines are not used as input for DEM generation, so they are an independent check of the accuracy of the DEM. The "sample" function in R was used to randomly select 1,000 points, and the root mean square error was determined to be 0.056 m (~0.18 ft). The $\sigma z_{2022,DEM}$ term is ignored in GCD uncertainty estimation because the comparison is made between MBMS point datasets having similar raw point densities that are ultimately gridded to the same extent and cell resolution.

When the values $\sigma z_{2022,datum} = 0.015$ m (~0.049 ft) and $\sigma z_{2022,DEM} = 0.056$ m (~0.18 ft) are substituted into equation 4 as constants, the uncertainty in storage capacity compounds with water-surface elevations associated with larger reservoir areal extents. Table 1 shows the uncertainty in storage capacity at the 95-percent confidence level, which generally increases with increasing water-surface elevation.

Storage Capacity Change

Storage capacities were compared between the 2012 tabulated estimates made by Lee (2013) and the 2022 estimates computed from the integrated 2022 bathymetric and multisource datasets (section "Contour Map Generation and Storage Capacity Estimation"). The storage capacity change, Δs_{WSEL} shown in equation 5 was computed for each water-surface elevation:

$$\Delta s_{WSEL} = s_{2022[WSEL]} - s_{2012[WSEL]}, \tag{5}$$

where

- $s_{2012[WSEL]}$ is the storage capacity in 2012 from Lee (2013) for a given water-surface elevation, and
- $s_{2022[WSEL]}$ is the storage capacity in 2022 for the same water-surface elevation.

Additionally, equation 6 shows the formulation for the percent change in storage capacity for a given water-surface elevation increment, L_{WSEL}, following Rahmani and others (2018):

$$L_{WSEL} = 100 \times \frac{\Delta s_{WSEL}}{s_{2012[WSEL]}}. \tag{6}$$

Storage capacity change and percent change could not be computed for water-surface elevations not previously estimated by Lee (2013), particularly those made at 0.50-m increments and (or) greater than the normal pool elevation. Results for Δs_{WSEL} and L_{WSEL} indicate minimal to no storage capacity losses, with nearly identical storage capacities between surveys (fig. 6). Reductions in storage capacity since 2012 ($L_{WSEL} < 0$) are observed for three of the water-surface elevations, including the normal pool elevation (table 1).

For discussion purposes, v_{net} for A_{RP} (table 2) is analogous to the storage capacity change computed for the 222.50-m (729.99-ft) water-surface elevation (table 1) because the reservoir area with elevations below that closely approximates the reservoir area analyzed by means of GCD. A gain in storage capacity is observed for the 222.50-m (729.99-ft) water-surface elevation, whereas the positive net change from the GCD analysis would indicate a slight loss in storage capacity for the same area. The opposite results stem from the removal of presumed 2012 TIN interpolation artifacts during data preparation for GCD analysis (section "Data Preparation"), whereas original estimates from Lee (2013) were utilized in the computation of storage capacity change (eq. 5). More importantly, the contrast reflects the magnitude of the real storage capacity change in Randy Poynter Lake being too small to detect with respect to reasonable uncertainty bounds.

Uncertainty in the percent change in storage capacity was not computed because $\sigma s_{2022} > \Delta s_{WSEL}$ for all increments of water-surface elevation (table 1). Despite the change being less than the uncertainty, the consistent gains in storage capacity for most water-surface elevations could be indicative of a systematic bias or process that causes elevations in the 2022 DEM to be lower, on average, than elevations in the 2012 TIN. For example, storage capacity gains may be an artifact of different post-processing procedures applied to the 2012 and 2022 MBES data; upright trees were removed from the 2022 data (section "Bathymetric Data Post-Processing"), whereas Lee (2013) may have included more upright trees (higher elevation points) in the post-processed MBES data. As mentioned previously, TIN interpolation artifacts identified in the 2012 surface could also systematically bias the results. Alternatively, compaction leads to a post-depositional decrease in the thickness of accumulated sediments that can continue to decrease over time (Maier and others, 2013), and this process may have caused a true lowering of the 2022 DEM as compared to the 2012 DEM, especially if the rate of compaction was faster than the rate of sediment accumulation between 2012 and 2022. Regardless, the presence or absence of a systematic bias is indeterminable within the scope of this study; therefore, it is necessary to reiterate the importance of discussing the computed storage capacity change with respect to uncertainty.

Potential Implications to Reservoir Life

Results from both the storage capacity change (normal pool elevation, table 1) and GCD analysis (v_{net} for A_{RP}, table 2) revealed storage capacity loss in Randy Poynter Lake. Future impacts of sedimentation on storage capacity loss are assessed by computing the reservoir half-life, $t_{1/2}$, the year that half of the reservoir is expected to be infilled with sediment. The half-life is formulated by equation 7 (Rahmani and others, 2018):

$$t_{\frac{1}{2}} = t_0 + \frac{s_0 / SY \times A_W}{2}, \tag{7}$$

where

- t_0 is the year associated with the most recent storage capacity estimate;
- s_0 is the storage capacity estimate at t_0, in units of length (L) cubed;
- SY is sediment yield, in units of L³/L²/year; and
- A_W is the watershed area, in units of L², that contributes sediment to the reservoir.

As equation 7 shows, half-life depends on the estimation of sediment yield, defined as the total amount of material per unit area reaching a point of interest over a specific period from sediment transport. Sediment yield is usually expressed in units of cubic meters per square kilometer per year, and its computation involves several steps, but a generalized formulation is given by equation 8 (Rahmani and others, 2018):

$$SY = \frac{v_{total}}{T} / A_W\,. \tag{8}$$

In the context of Randy Poynter Lake, v_{total} in equation 8 is the total volume of sediment that reaches Randy Poynter Lake (units of L³), T is the time period in years between repeat MBES surveys, A_W is the watershed area upstream of the outflow location of Randy Poynter Lake at Jack Turner Dam (fig. 3), and v_{total} is approximated from the volumetric change results of this study. Equation 8 excludes the amount of sediment that passed downstream from Jack Turner Dam for simplicity.

First, equation 9 is used to determine v_{total}; the simple formulation in equation 9 assumes all sediment exported upstream of the outflow location was trapped within the flood pool areal extent of Randy Poynter Lake, such that v_{total} is the sum of the measured volume from the GCD analysis, v_{meas}, and any unmeasured volume change, $v_{unknown}$:

$$v_{total} = v_{meas} + v_{unknown}\,. \tag{9}$$

Measured volume change is derived from either v_{net} or v_{dep} for A_{RP} (table 2). The $v_{unknown}$ term is included because the GCD analysis excludes potentially trapped sediment in the remaining 23.37 percent of the flood pool extent not analyzed by means of GCD, composed mostly of shoreline areas. Sediment accumulation in the unmeasured area is not likely negligible, especially near the inflow location of Big Haynes Creek where satellite imagery shows the formation of subaerial deltaic deposits (fig. 7*C*).

Next, $v_{unknown}$ was determined to account for storage capacity loss in the unmeasured areas within the flood pool. As implied, it is unknown how much change occurred there, but it can be approximated with $v_{delivered}$, the volume of sediment delivered to Randy Poynter Lake between the repeat MBES surveys. The value for $v_{delivered}$ is approximated from previous estimates of sediment load—the sediment a stream transports and delivers. Aulenbach and others (2023a) used a regression-model approach to estimate load between October 1, 2010, and September 30, 2020, from suspended sediment concentration measured at the USGS gaging station located on Big Haynes Creek (site 02207385), approximately 15.4 kilometers (~9.57 miles) upstream of Jack Turner Dam. Sediment load estimates for other streams that discharge into Randy Poynter Lake are not available; however, their contribution is assumed as negligible compared to Big Haynes Creek. Mean daily flux from Aulenbach and others (2023b) was multiplied by the time, in days, between repeat MBES surveys, assuming the mean daily flux for the period between September 30, 2020, and the 2022 MBES survey equates to the reported 2010–20 rate. Ignoring the contribution from bedload transport, which is also unknown, the resulting total study period load was converted to a volume using a bulk density of 1.1 tons per cubic meter following Renwick and others (2005), and $v_{delivered}$ was determined to be 92,511 cubic meters (m³) (~75.00 acre-feet). The approximation is limited by the availability of sediment load estimates representative of a point directly upstream of Randy Poynter Lake, as sediment load could increase or decrease downstream from the gaging location.

Reservoir half-life was estimated for the following three SY scenarios derived from different values of v_{tot} (eq. 9) to demonstrate the impact of stated assumptions:

Scenario 1: $v_{meas} = v_{dep}$ and $v_{unknown} = v_{delivered}$,

Scenario 2: $v_{meas} = v_{net}$ and $v_{unknown} = v_{delivered}$,

Scenario 3: $v_{meas} = v_{net}$ and $v_{unknown} = 0$.

Both scenarios 1 and 2 assert $v_{unknown} = v_{delivered}$, such that all sediment delivered to Randy Poynter Lake was deposited in the unmeasured area, although it is likely that a portion of $v_{delivered}$ is at least partially encompassed by v_{meas}, given the relatedness of increased deposition with the inflow location of Big Haynes Creek (fig. 4; section "Bathymetric Change and Difference Map"). Use of v_{dep} in scenario 1 as compared to v_{net} in scenario 2 explicitly ignores measured storage capacity gains (v_{ero}, table 2), and the former will likely produce an overestimation of SY and ultimately a more conservative (earlier in time) reservoir half-life. For the least conservative estimate, it is assumed in scenario 3 that all accumulated sediment upstream from the dam was already measured in the GCD analysis. All scenarios use the values of $A_W = 121.99$ km² (~47.10 mi²), $t_0 = 2022$, and $s_0 = 24{,}426{,}826$ m³, which represent the watershed area upstream from the outflow location of Randy Poynter Lake determined from the USGS StreamStats web application (U.S. Geological Survey, 2023b), the year of the bathymetry survey, and the 2022 estimate for the storage capacity at the flood pool elevation from table 1, respectively. The results for each scenario are as follows:

Scenario 1: $SY = 79.92$ m³/km²/yr

$t_{1/2} = 2669$, or 647 years from 2022

Scenario 2: $SY = 154.74$ m³/km²/yr

$t_{1/2} = 3274$, or 1,252 years from 2022

Scenario 3: $SY = 6.34$ m³/km²/yr

$t_{1/2} = 17794$, or 15,782 years from 2022.

Although sediment is accumulating in Randy Poynter Lake near the inflow location of Big Haynes Creek, the reservoir-wide GCD analysis demonstrates most of Randy Poynter Lake is not subject to the same magnitude of deposition (fig. 4), which implies the study-area averaged change is the most appropriate basis for determining reservoir half-life (scenario 2). Scenario 2 conservatively estimates reservoir half-life of Randy Poynter Lake to extend more than 1,000 years beyond the reported end-of-use date in 2030 (Rockdale Water Resources, 2023). Importantly, SY is a constant in the formulation for sediment yield and therefore assumes the factors that affect storage capacity change will have the same cumulative effect in the future as those measured in the decade between 2012 and 2022. However, the factors that affect storage capacity are not constant; for example, sediment delivery may tend to increase, land use and sediment management practices in the surrounding drainage basin may change, rainfall-runoff patterns could change, and sediment compaction rates may increase or decrease (Schleiss and others, 2016). The change measured between repeat bathymetric surveys of Randy Poynter Lake promotes an understanding of decadal-scale rates of storage loss that any future monitoring efforts can leverage to better determine the long-term rates and document the timewise variability of storage loss (Morris, 2015) for more accurate reservoir lifetime forecasts.

References Cited

Anderson, S.W., 2018, Uncertainty in quantitative analyses of topographic change—Error propagation and the role of thresholding: Earth Surface Processes and Landforms, v. 44, no. 5, p. 1015–1033, accessed January 15, 2024, at https://doi.org/10.1002/esp.4551.

Aulenbach, B.T., Henley, J.C., and Hopkins, K.G., 2023a, Hydrology, water-quality, and watershed characteristics in 15 watersheds in Gwinnett County, Georgia, water years 2002–20: U.S. Geological Survey Scientific Investigations Report 2023–5035, 106 p., accessed January 15, 2024, at https://doi.org/10.3133/sir20235035.

Aulenbach, B.T., Henley, J.C., and Hopkins, K.G., 2023b, Watershed characteristics and streamwater constituent load data, models, and estimates for 15 watersheds in Gwinnett County, Georgia, 2000–2021: U.S. Geological Survey data release, accessed January 15, 2024, at https://doi.org/10.5066/P9G8HZTY.

Blue Marble Geographics, 2023, Global Mapper (ver. 23): Blue Marble Geographics software release, accessed January 23, 2023, at https://www.bluemarblegeo.com/.

Bolton, W.J., and Whaling, A.R., 2023, Bathymetric and supporting data for estimation of reservoir storage capacity and geomorphic change detection analysis from a multibeam bathymetric survey of Randy Poynter Lake, Rockdale County, Georgia: U.S. Geological Survey data release, https://doi.org/10.5066/P9G9YVDU.

Calder, B.R., and Wells, D.E., 2007, CUBE user's manual: Durham, N.H., University of New Hampshire, Center for Coastal and Ocean Mapping, 54 p., accessed April 26, 2023, at https://scholars.unh.edu/ccom/1217.

Coleman, J.M., and Wright, L.D., 1975, Modern river deltas—Variability of processes and sand bodies, in Broussard, M.L., ed., Deltas—Models for exploration: Houston, Tex., Houston Geological Society, p. 99–149.

Elliott, T., 1986, Deltas, chap. 6 of Reading, H.G., ed., Sedimentary environments and facies (2d ed): Oxford, U.K., Blackwell, p. 113–154.

Esri, 1998, Esri shapefile technical description: Environmental Systems Research Institute, accessed May 1, 2023, at https://www.esri.com/content/dam/esrisites/sitecore-archive/Files/Pdfs/library/whitepapers/pdfs/shapefile.pdf.

Ghoshal, S., James, L.A., Singer, M.B., and Aalto, R., 2010, Channel and floodplain change analysis over a 100-year period—Lower Yuba River, California: Remote Sensing, v. 2, no. 7, p. 1797–1825, accessed January 15, 2024, at https://doi.org/10.3390/rs2071797.

Hijmans, R., 2023, Package 'terra'—Spatial data analysis (ver. 1.7–39): Comprehensive R Archive Network [CRAN] web page, accessed September 2023 at https://cran.r-project.org/web/packages/terra/terra.pdf.

Huizinga, R.J., 2017, Bathymetric and velocimetric surveys at highway bridges crossing the Missouri and Mississippi Rivers near St. Louis, Missouri, May 23–27, 2016: U.S. Geological Survey Scientific Investigations Report 2017–5076, 102 p., accessed November 15, 2023, at https://doi.org/10.3133/sir20175076.

International Hydrographic Organization, 2020, IHO standards for hydrographic surveys, edition 6.0.0: International Hydrographic Organization Special Publication, S–44, 41 p., accessed November 15, 2023, at https://doi.org/10.25607/OBP-1354.2.

James, A.L., Hodgson, M.E., Ghoshal, S., and Latiolais, M.M., 2012, Geomorphic change detection using historic maps and DEM differencing—The temporal dimension of geospatial analysis: Geomorphology, v. 137, no. 1, p. 181–198, accessed January 15, 2024, at https://doi.org/10.1016/j.geomorph.2010.10.039.

Lee, K.G., 2013, Estimation of reservoir storage capacity using multibeam sonar and terrestrial lidar, Randy Poynter Lake, Rockdale County, Georgia, 2012: U.S. Geological Survey Scientific Investigations Map 2013–3265, 1 sheet, scale 1:100,000, accessed January 15, 2024, at https://doi.org/10.3133/sim3265.

Maier, D.B., Rydberg, J., Bigler, C., and Renberg, I., 2013, Compaction of recent varved lake sediments: GFF, v. 135, nos. 3–4, p. 231–236, accessed January 15, 2024, at https://doi.org/10.1080/11035897.2013.788551.

Morris, G.L., 2015, Collection and interpretation of reservoir data to support sustainable use, in Joint Federal Interagency Conference [5th Federal Interagency Hydrologic Modeling Conference and the 10th Federal Interagency Sedimentation Conference], Reno, Nevada, April 19–23, 2015, [Proceedings]: SEDHYD, p. 1659–1668, accessed January 15, 2024, at https://www.academia.edu/26657621/COLLECTION_AND_INTERPRETATION_OF_RESERVOIR_DATA_TO_SUPPORT_SUSTAINABLE_USE.

National Geodetic Survey, 2022, OPUS—Online Positioning User Service: National Geodetic Survey web page, accessed December 12, 2022, at https://www.ngs.noaa.gov/OPUS/.

Queen, A., 2022, Silt collecting in Randy Poynter Lake a growing concern: The Citizens [Newton, Rockdale], September 6, 2021, accessed January 15, 2024, at https://www.rockdalenewtoncitizen.com/news/silt-collecting-in-randy-poynter-lake-a-growing-concern/article_5ee948b8-0cd0-11ec-a3bb-d7f64d11a337.html.

Rahmani, V., Kastens, J.H., DeNoyelles, F., Jakubauskas, M.E., Martinko, E.A., Huggins, D.H., Gnau, C., Liechti, P.M., Campbell, S.W., Callihan, R.A., and Blackwood, A.L., 2018, Examining storage capacity loss and sedimentation rate of large reservoirs in the central U.S. Great Plains: Water, v. 10, no. 2, 190 p., accessed January 15, 2024, at https://doi.org/10.3390/w10020190.

R Core Development Team, 2023, R—A language and environment for statistical computing (ver. 4.3.1): Vienna, Austria, R Foundation for Statistical Computing software release, accessed December 18, 2023, at https://www.R-project.org.

Renwick, W.H., Smith, S.V., Bartley, J.D., and Buddemeier, R.W., 2005, The role of impoundments in the sediment budget of the conterminous United States: Geomorphology, v. 71, nos. 1–2, p. 99–111, accessed January 15, 2024, at https://doi.org/10.1016/j.geomorph.2004.01.010.

Rockdale Water Resources, 2023, Randy Poynter Lake and Jack Turner Dam: Rockdale Water Resources web page, accessed September 25, 2023, at https://www.rockdalewaterresources.com/reservoir.

Roussel, J.-R., and Auty, D., 2023, Package 'lidR'—Airborne LiDAR data manipulation and visualization for forestry applications (ver. 4.0.3): Comprehensive R Archive Network [CRAN] web page, accessed September 25, 2023, at https://cran.r-project.org/web/packages/lidR/lidR.pdf.

Rydlund, P.H., Jr., and Densmore, B.K., 2012, Methods of practice and guidelines for using survey-grade global navigation satellite systems (GNSS) to establish vertical datum in the United States Geological Survey: U.S. Geological Survey Techniques and Methods, book 11, chap. D1, 102 p. [Also available at https://doi.org/10.3133/tm11D1.]

Schleiss, A.J., Franca, M.J., Juez, C., and De Cesare, G., 2016, Reservoir sedimentation: Journal of Hydraulic Research, v. 54, no. 6, p. 595–614, accessed January 15, 2024, at https://doi.org/10.1080/00221686.2016.1225320.

Trimble Applanix, 2022, POSPac Mobile Mapping Suite (MMS) 8.9: Applanix Corporation software release, accessed October 17, 2022, at https://www.applanix.com/products/pospac-mms.htm.

U.S. Army Corps of Engineers, 2013, Hydrographic surveying: U.S. Army Corps of Engineers, Engineer Manual 1110–2–1003, 699 p., accessed January 15, 2024, at https://www.publications.usace.army.mil/Portals/76/Publications/EngineerManuals/EM_1110-2-1003.pdf?ver=gDGVUj_0XR2sXHiIpQZv2Q%3d%3d.

U.S. Geological Survey, 2023a, 3D elevation program lidar point cloud (published July 2021): U.S. Geological Survey web page, accessed September 1, 2022, at https://www.usgs.gov/the-national-map-data-delivery.

U.S. Geological Survey, 2023b, StreamStats: U.S. Geological Survey web page, accessed December 18, 2023, at https://streamstats.usgs.gov/ss/.

Wheaton, J.M., Brasington, J., Darby, S.E., and Sear, D.A., 2010, Accounting for uncertainty in DEMs from repeat topographic surveys—Improved sediment budgets: Earth Surface Processes and Landforms, v. 35, no. 2, p. 136–156, accessed January 15, 2024, at https://doi.org/10.1002/esp.1886.

Xylem, Inc., 2022, HYPACK 2022: Xylem, Inc., software release, accessed October 17, 2022, at https://www.xylem.com/en-us/brands/hypack/.

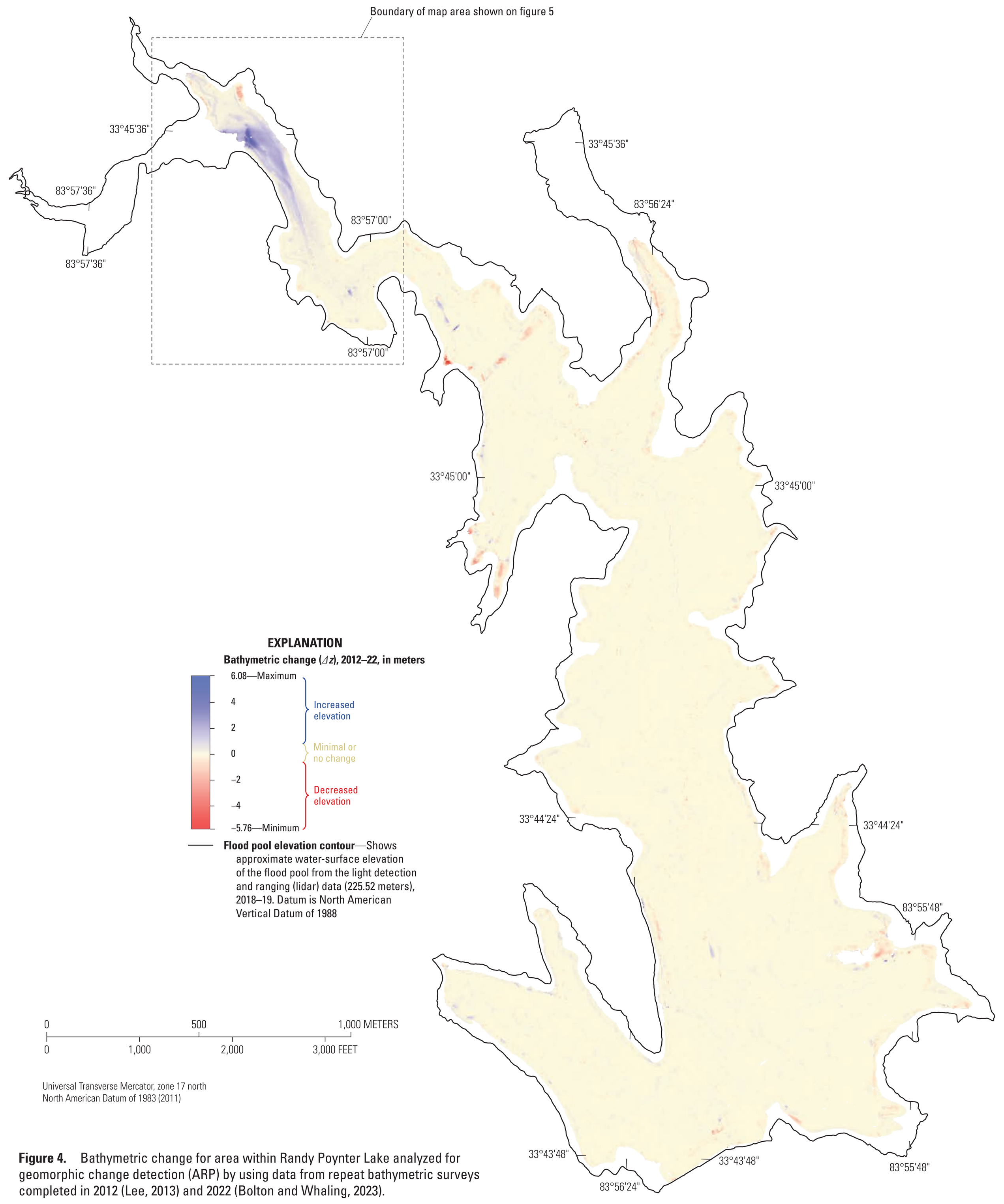

Figure 4. Bathymetric change for area within Randy Poynter Lake analyzed for geomorphic change detection (ARP) by using data from repeat bathymetric surveys completed in 2012 (Lee, 2013) and 2022 (Bolton and Whaling, 2023).

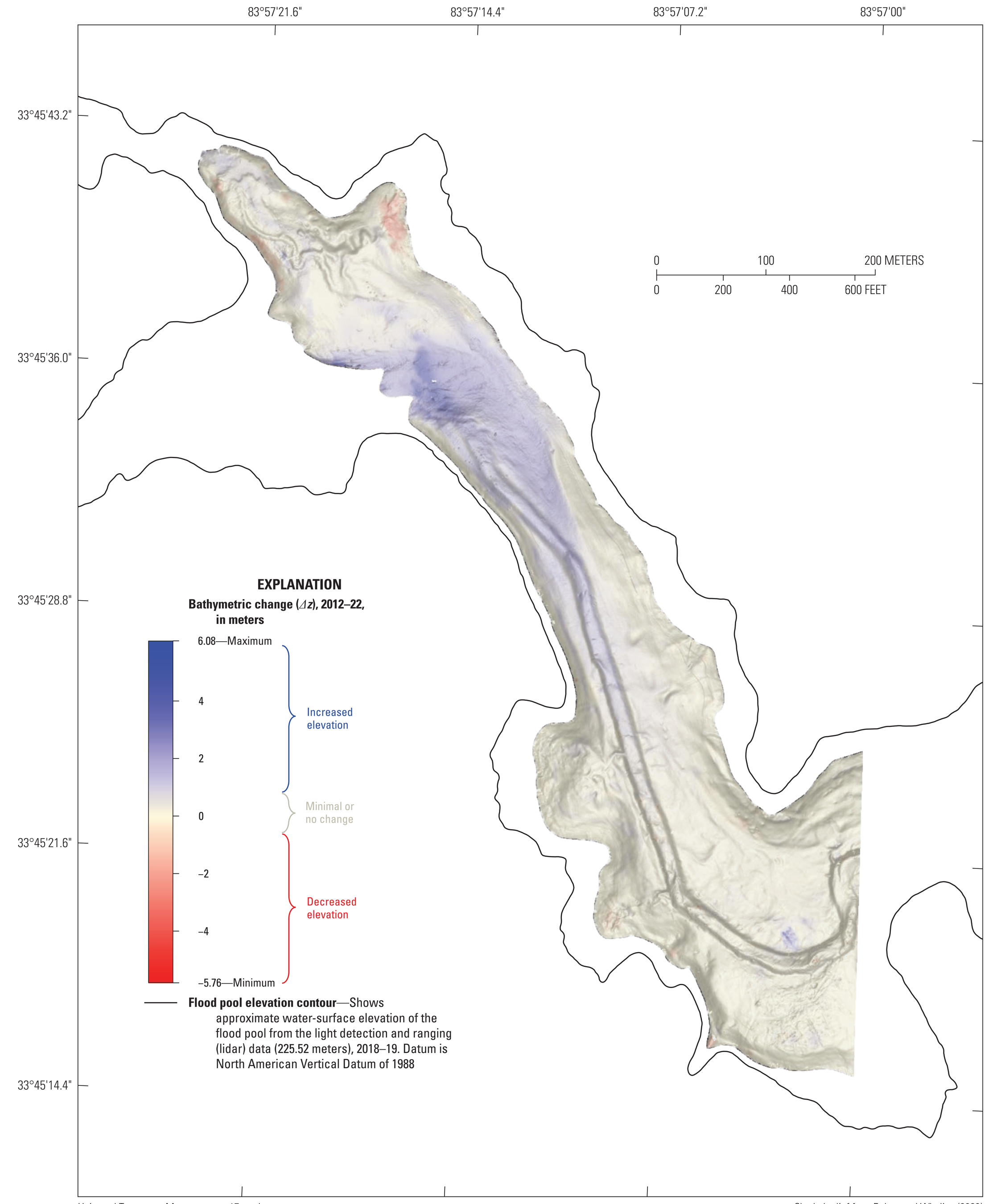

Figure 5. Bathymetric change map of Big Haynes Creek subarea within Randy Poynter Lake (ABH) by using data from repeat bathymetric surveys completed in 2012 and 2022. The bathymetric change is displayed with a transparency to reveal a shaded relief digital elevation model (DEM) that was generated primarily from 2022 bathymetric survey data.

Table 2. Bathymetric change and uncertainty for the entire area within Randy Poynter Lake analyzed for geomorphic change detection (A_{RP}) and for the area near the inflow location of Big Haynes Creek (A_{BH}).

[GCD, geomorphic change detection; %, percent; <, less than]

Geomorphic change detection metric	*n* (number of grid cells analyzed)	Volume change (*v*), in cubic meters	Volume uncertainty (σv), in cubic meters (95% confidence level)	Volume change (*v*), in acre-feet	Volume uncertainty (σv), in acre-feet (95% confidence level)	Volume change as percentage of 2022 normal pool storage capacity	Volume uncertainty as percentage of 2022 normal pool storage capacity
Entire area analyzed for GCD (A_{RP})							
Net change, v_{net}	8,889,368	7,976.28	92,400.27	6.47	74.91	0.04	0.45
Positive change, v_{dep} (deposition)	3,846,910	102,040.53	39,986.59	82.73	32.42	0.50	0.20
Negative change, v_{ero} (erosion)	5,039,035	−94,064.25	52,378.10	−76.26	42.46	0.46	0.26
Big Haynes Creek subarea of interest (A_{BH})							
Net change, v_{net}	512,418	48,719.11	30,981.26	39.50	25.12	0.24	0.15
Positive change, v_{dep} (deposition)	454,083	51,721.88	4,719.95	41.93	3.83	0.25	0.02
Negative change, v_{ero} (erosion)	58,290	−3,002.78	605.89	−2.43	0.49	0.01	<0.01

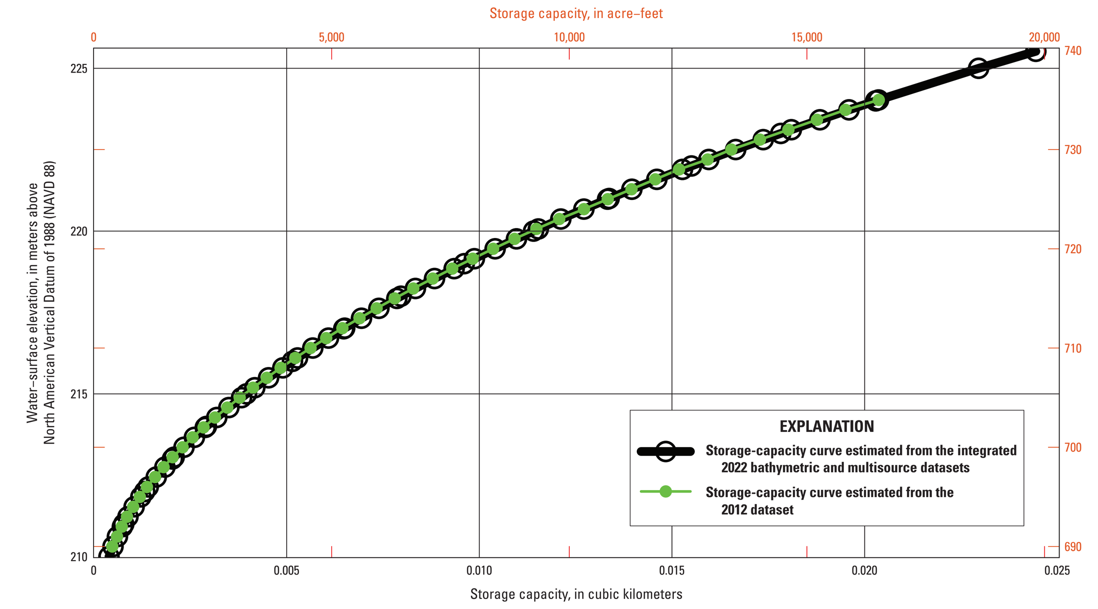

Figure 6. Relation between water-surface elevation and storage capacity for Randy Poynter Lake in 2012 from tabulated estimates made by Lee (2013) and in 2022 derived from a continuous digital elevation model (DEM). Data used to generate the DEM primarily originate from the 2022 bathymetric survey and are available in Bolton and Whaling (2023).

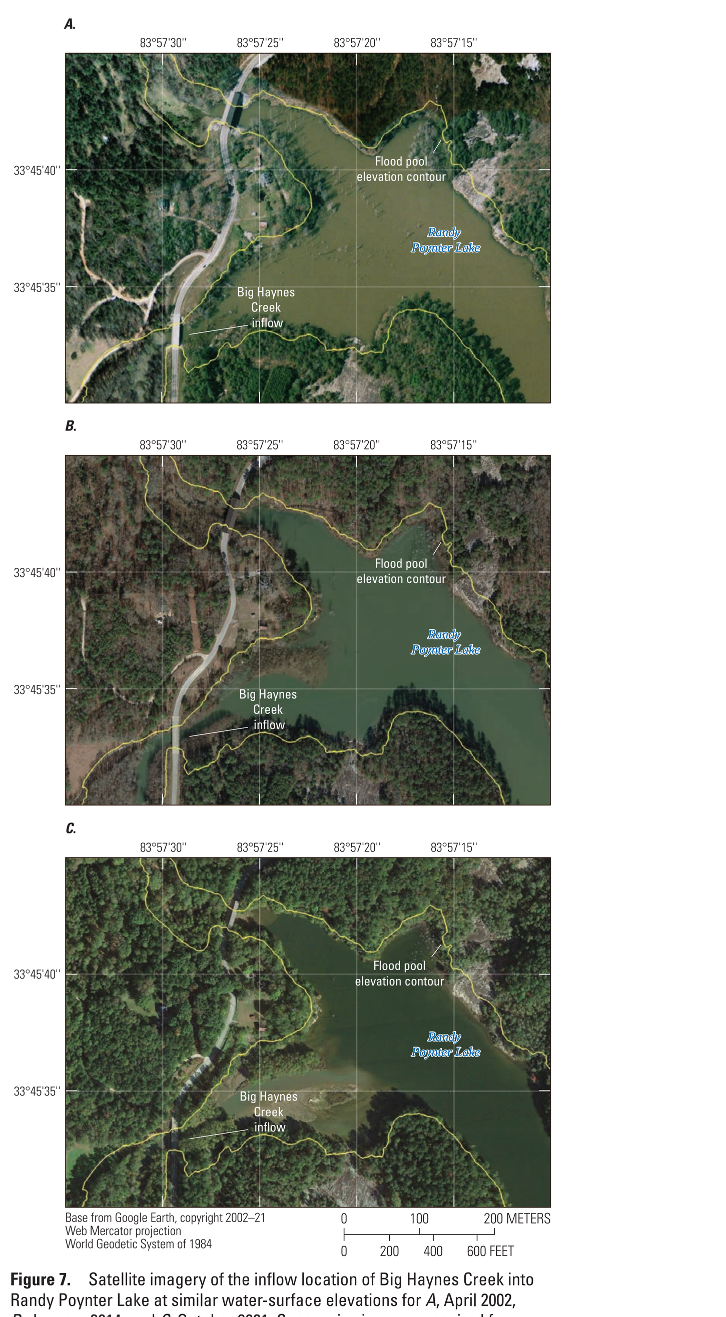

Figure 7. Satellite imagery of the inflow location of Big Haynes Creek into Randy Poynter Lake at similar water-surface elevations for *A*, April 2002, *B*, January 2014, and *C*, October 2021. Successive imagery acquired from Google Earth shows formation of subaqueous deposits that resemble a delta.

Estimation of Reservoir Storage Capacity and Geomorphic Change Detection Analysis From a Multibeam Bathymetric Survey of Randy Poynter Lake, Rockdale County, Georgia

By

Amanda R. Whaling and Wesley J. Bolton

2024

Digital files available at https://doi.org/10.3133/sim3523

Suggested citation: Whaling, A.R., and Bolton, W.J., Estimation of reservoir storage capacity and geomorphic change detection analysis from a multibeam bathymetric survey of Randy Poynter Lake, Rockdale County, Georgia: U.S. Geological Survey Scientific Investigations Map 3523, 2 sheets, https://doi.org/10.3133/sim3523.

Associated data for this publication: Aulenbach, B.T., Henley, J.C., and Hopkins, K.G., 2023, Watershed characteristics and streamwater constituent load data, models, and estimates for 15 watersheds in Gwinnett County, Georgia, 2000–2021: U.S. Geological Survey data release, https://doi.org/10.5066/P9G8HZTY.

Bolton, W.J., and Whaling, A.R., 2023, Bathymetric and supporting data for estimation of reservoir storage capacity and geomorphic change detection analysis from a multibeam bathymetric survey of Randy Poynter Lake, Rockdale County, Georgia: U.S. Geological Survey data release, https://doi.org/10.5066/P9G9YVDU.

ISSN 2329-132X (online)
https://doi.org/10.3133/sim3523